Enhancing analytical merits of laser-induced breakdown spectroscopy of hydrogen isotopes using an orthogonal double-pulsing scheme

Elizabeth J. Kautz[a,b,*], Mathew P. Polek[a,c], Ewa C.E. Rönnebro[a], Sivanandan S. Harilal[a,d,**]

[a]*Pacific Northwest National Laboratory, Richland, Washington 99352, USA*
[b]*North Carolina State University, Raleigh, North Carolina 27695, USA*
[c]*University of California San Diego, La Jolla, California 92093, USA*
[d]*Washington State University, Pullman, WA 99164, USA*

Abstract

Accurate detection and quantification of hydrogen isotopes in solid materials are vital for diverse applications, including fusion energy, hydrogen storage, and tritium production. Laser-induced breakdown spectroscopy (LIBS) is a well-established, rapid, standoff method for this purpose, but it faces challenges related to the analytical merits required for isotopic analyses. In this study, we enhance the analytical and detection capabilities of traditional single-pulse LIBS by implementing an orthogonal double pulsing approach, focusing on the analysis of a range of ^{2}H concentrations in Zircaloy-4 substrates (acting as a proxy for ^{3}H). The double-pulse experiments employed an orthogonal re-heating configuration with two nanosecond Nd:YAG lasers. We systematically evaluated critical parameters affecting the signal intensity in double-pulse LIBS, including interpulse delay, ambient gas pressure, and heating laser energy. Our results demonstrate that employing an orthogonal double-pulse scheme significantly enhances $^{2}H_{\alpha}$ emission while minimizing line broadening and self-absorption, ultimately improving the technique's analytical capabilities.

Keywords: hydrogen isotopes, laser produced plasma, optical diagnostics, LIBS

1. Introduction

Several energy and defense applications demand technologies that can accurately detect and quantify hydrogen (H) and its isotopes, protium (^{1}H), deuterium (^{2}H), and tritium (^{3}H), in solid matrices. In molten salt reactors and magnetic confinement fusion devices (e.g., ITER), monitoring tritium production, transport, and retention is essential for safe operation and effective tritium management [1–5]. The deuterium-tritium reaction is also the basis for producing energy in future modular fusion power plants. Determining the amount of tritium produced during neutron irradiation of Tritium Producing Burnable Absorber Rod (TPBAR) components is also critical for defense applications [6, 7]. Further, robust detection technologies with standoff measurement capability are strongly desirable given the toxicity of tritium and the environments in which tritium may be located and needs to be monitored. For example, in off-gas systems of advanced reactors, several radionuclides may be present, and remote handling/sensing is needed [8]. In addition, remote or standoff sensing is also desirable for monitoring first wall components in fusion devices, to determine fuel retention in such components during shut-down or maintenance periods [1, 9].

Laser-induced breakdown spectroscopy (LIBS) is one of the few well-established methods capable of in-situ, standoff measurements of all elements and some isotopes, including ^{1,2,3}H [10, 11]. In the LIBS method, laser ablation (LA) is used as a sampling method to generate plasma from the target of interest. By analyzing the spontaneous emission from this laser-produced plasma (LPP), characteristic emission of plume species (e.g., atoms, ions, molecules) can indicate what elements are present in the target material. The applications of LIBS in the fields of nuclear nonproliferation and nuclear industry are well-documented [9, 10, 12–16]. While LIBS is widely used for elemental detection, isotopes from some elements can also be resolved, depending on detection equipment resolution and the isotopic shift. The isotopic shift for deuterium/protium is $\approx$ 180 pm, is even larger for tritium/protium ($\approx$ 240

*Corresponding author: ekautz@ncsu.edu
**Corresponding author: hari@pnnl.gov

pm) and hence these isotopes can be resolved with traditional laboratory-based high-resolution spectrographs if line broadening is minimized [17–20]. However, challenges arise when using LIBS for the detection/analysis of very low or very high (30 at. % and greater) concentrations of ^{1,2,3}H analytes. The detection limit of LIBS for H in the solid matrix is $\sim$ 10 ppm for ^{2}H [21]. A different challenge exists when trying to use LIBS for the analysis of high analyte concentrations; self-absorption may be present, owing to the high atom density of the analyte [22, 23]. To overcome such challenges, various methodologies can be employed including microwave-enhanced LIBS [24], laser-induced fluorescence (LIF) of LIBS [25], and double-pulse (DP) LIBS [19, 26]. Previously, a DP scheme was successfully used for enhancing emission features from LPPs for various applications including detecting explosives [27], analysis of aerosols [28], chemical analysis of seawater [29–31], soil analysis [32], carbon detection [33], improved chemical imaging [34], and monitoring hydrogen isotopes in the first wall of fusion devices [1, 4, 26].

One of the key advantages of LIBS is the large parametric space for optimization [10]. Compared to single-pulse (SP) LIBS, DP-LIBS is significantly more complex, given there are more parameters available for controlling plasma temporal evolution and emission spectral features [35]. While more complex, the larger parametric space in DP-LIBS can be advantageous for optimizing analytical merits relevant to hydrogen isotopic analysis. Key parameters in DP-LIBS experimental set-ups are the configuration of the two laser pulses, inter-pulse timing of the second laser beam relative to the first, and energies of the pre- and heating pulses. Several possible schemes exist for DP-LIBS, including collinear, orthogonal, and crossed-beam approaches [36]. The type of DP configuration selected is driven by the requirements of the application. From our prior work on the analysis of hydrogen isotopes via LIBS, we found that hydrogen isotope emission was strongest close to the target surface [17]. In addition, a previously developed calibration curve showed evidence of emission intensity saturating at high ^{2}H concentrations [22], indicative of self-absorption. Hence, preferential re-heating of the region of the LPP where the population of ^{2}H species is prominent (i.e., close to the target) and at later times when electron density is low could improve the analytical capabilities of LIBS over a wide ^{2}H concentration range.

Here, we compare results from single- and double-pulse LIBS to evaluate the impact of a DP scheme on improving signal enhancement and reducing self-absorption. We analyze several Zircaloy-4 target materials with varying ^{2}H concentrations, where ^{2}H is used as a proxy for ^{3}H. For DP experiments, an orthogonal configuration is used to selectively heat the region of the LPP where ^{2}H species population is prominent. This work aims to evaluate the impact of interpulse delay, heating laser energy, and ambient gas pressure, on signal enhancement, line broadening, and analytical capabilities of hydrogen isotopic analysis via LIBS.

2. Experimental Materials and Methods

Zircaloy-4 samples with varying ^{2}H concentrations were prepared using a custom-built Sievert's apparatus [22]. To absorb ^{2}H into a specimen, ^{2}H is first introduced from a gas pressure bottle into a calibrated volume to a desired pressure and thereafter, the known gas volume and pressure of $^{2}H_2$ are introduced into an attached autoclave. The ^{2}H content being absorbed into specimens is calculated by measuring the pressure drop relative to the calibrated volume, which allows for in situ monitoring of ^{2}H pick-up. The specimens are also weighed before and after ^{2}H absorption on an analytical balance ($\pm$0.1 mg) to confirm absorbed wt.% of ^{2}H. The Zircaloy-4 tubular specimens analyzed in this work were 50 mm long with an outer diameter of $\approx$ 5 mm, and thickness of $\approx$ 300 μm. All ^{2}H absorption procedures were performed at 500 °C. Zircaloy-4 specimens with the following estimated concentrations were prepared using the methods described here: 5.5, 16, 27, 33, 41, and 47 at. % ^{2}H. In addition to ^{2}H, the Zircaloy-4 target contained $\approx$ 10 ppm ^{1}H. ^{1}H from the environment (contamination) is also expected on the surface of the Zircaloy-4 targets.

The experimental set-up for plasma generation and data collection is schematically described in Figure 1(a). Target materials for analysis were loaded into a cubic vacuum chamber, which contained a gas manifold, vacuum pump and vacuum gauge for controlling/measuring ambient gas and pressure. This chamber was placed on an x-y stage to move between targets and prevent drilling. In this work, all experiments were performed in flowing He gas. The experimental scheme consisted of two nanosecond (ns) Nd:YAG lasers (Continuum Surelite, 1064 nm, 6 ns full-width half maximum (FWHM)). Laser energies of both beams were attenuated using a combination of half waveplate and cube polarizer. An orthogonal double pulse scheme was used in the present study. Here the first laser pulse was used to ablate the sample and create a plasma by focusing the beam using a planoconvex lens (f = 15 cm). The spot size at the target was $\approx$500 μm. The second laser was propagated

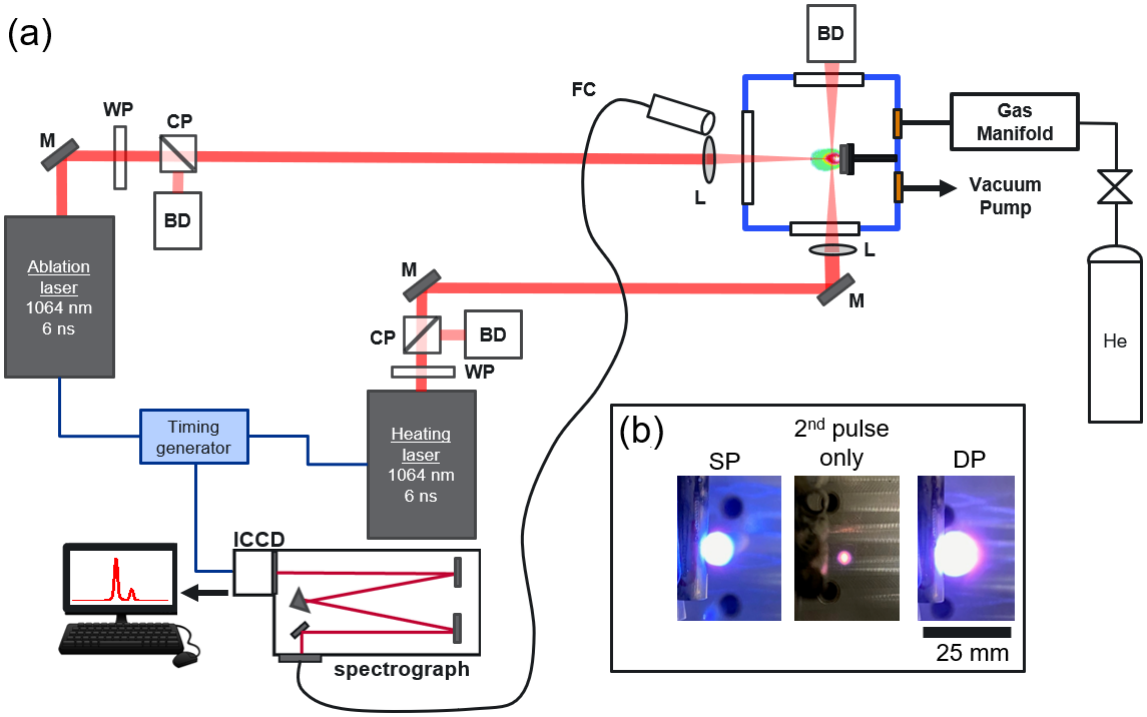

Figure 1: (a) Experimental set-up used for LIBS employing single pulse (SP) and double pulse (DP) schemes. Abbreviations are defined as follows: M (mirror), L (focusing lens), BD (beam dump), WP (wave plate), CP (cube polarizer), FC (fiber cable), ICCD (intensified charged coupled device). (b) Time-integrated photographs of plasmas generated by: (left) ablation pulse (i.e., SP), (middle) the orthogonal reheating pulse only (He breakdown plasma), and (right) double-pulse schemes (both ablation and reheating pulses combined).

orthogonal to the first laser and was used for generating a He breakdown plasma just above the target ($\approx$ 1.5 mm away) by focusing using a planoconvex lens (f = 15 cm). The breakdown He plasma was used to reheat the Zirclaoy plasma without interacting with the target.

Time-integrated images of various plasmas (SP, He breakdown plasma and DP) were obtained using a CCD camera are also given in Figure 1(b). In addition to time-integrated images, time-resolved filtered imaging of the single plasmas was carried out by positioning an intensified CCD (PIMAX Princeton Instruments) orthogonal to the plasma expansion direction. A narrow band pass filter (656.3 nm $\pm$ 1 nm bandwidth) was positioned in front of the camera to map the distribution of $^2H_\alpha$ and $^1H_\alpha$ species in the plasma.

Optical emission spectroscopy (OES) was performed to measure H isotopic splitting and intensity in a spatially integrated manner. For performing OES, the UV-VIS emission from the plasma was transported to a 0.75 m spectrograph (SpectraPro HRS-750, Princeton Instruments) equipped with an intensified CCD (ICCD, PI-MAX4, Princeton Instruments) using a 19-core fiber bundle cable oriented $\approx$20° relative to the target normal. A 2400 grooves/mm grating was used for all data collection that provided a spectral resolution of $\approx$ 0.013 nm at FWHM measured using a He-Ne laser at 632 nm. A digital timing delay generator was used to control the timing between the first pulse, heating pulse, delay, and gate width of detection. The emission intensity (i.e., peak area) and FWHM of $^2H_\alpha$ spectral profiles are measured using a Voigt fit.

3. Results

3.1. Single pulse plasma characterization

Our previous results showed the presence of self-absorption in H_α transition for samples containing high analyte concentration [22]. Two commonly used methods for minimizing self-absorption are using reduced pulse energy for ablation and reduced background pressures. Therefore, thee laser ablation of Zircaloy-4 target was carried out using a laser energy of 50 mJ. Our previous studies highlighted that a flowing inert gas (Ar, He) at reduced pressure levels provided narrow

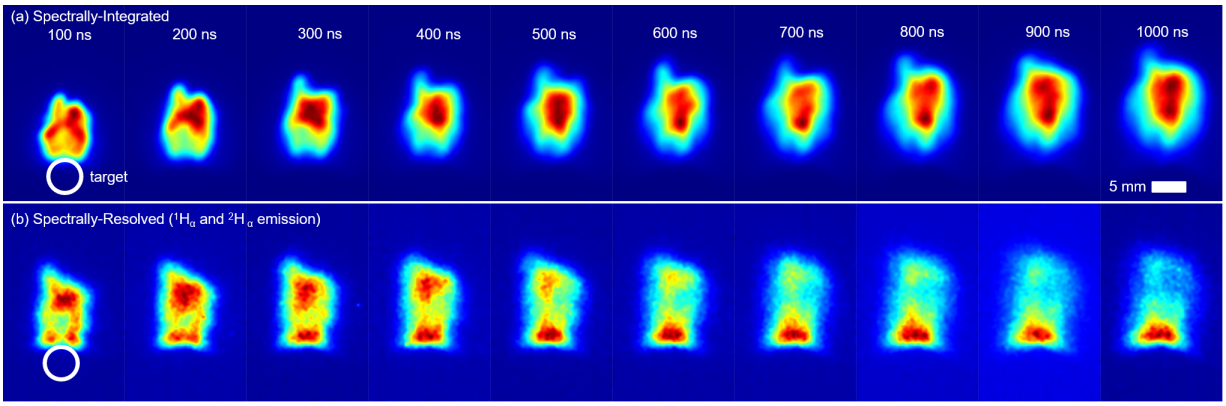

Figure 2: (a) Spectrally-integrated, and (b) spectrally-resolved images of LPPs generated from a ^{2}H-loaded Zircaloy-4 target material. The plasma images were collected using an ICCD. For recording spectrally-resolved images, a narrowband filter was placed in front of the ICCD that only transmitted light from $^1H_\alpha$ and $^2H_\alpha$ transitions. The experiment was performed using 50 mJ ablation laser energy and at an ambient He pressure of 75 Torr. Gate delays are noted on each spectrally-integrated image. For spectrally-integrated images, progressive gating from 20 - 100 ns was used for gate delays ranging from 100 - 1000 ns. For spectrally-resolved images, a constant gate width of 300 ns was used.

H_α linewidth with a good signal-to-noise ratio (SNR) [17, 22]. Hence, in the present studies, the chamber pressure was maintained in the range of 30-100 Torr He.

To understand the spatial distribution of ^{2}H species and plume morphology, time-resolved, spectrally-integrated, and spectrally-resolved 2D images were taken by positioning an ICCD camera orthogonal to the plasma expansion direction, with results given in Figure 2. The He background pressure used was 75 Torr. The gate delays for each set of images are noted in Figure 2(a). The Zircaloy-4 sample contained $^2H \approx 1.09$ wt.%. The time-resolved images given in Figure 2 show that excited state ^{1,2}H distribution is primarily concentrated closer to the target surface. This trend is more significant at 500 ns and greater times after plasma onset. Plume splitting was also evident in the spectrally-resolved images in Figure 2(b).

Time-resolved, spatially-integrated spectral features were collected using the SP experimental configuration to evaluate $^2H_\alpha$ emission intensity and linewidth evolution. Results are reported in Figure 3, where all measurements were collected in a He ambient gas environment of 75 Torr. The sample used here is the same one used for imaging (Figure 2). Progressive gating was used for time-resolved measurements, with gate widths from 2 - 10 μs for gate delays of 1 - 30 μs. The spectral features (Figure 3(a)) showed the presence of both $^2H_\alpha$ and $^1H_\alpha$. Note that we used several cleaning shots before taking the data to remove the surface contamination, so the ^{1}H measured was not due to surface contamination. We attribute the ^{1}H signal to ^{1}H present in the Zircaloy-4 target material as a minor impurity element. The time evolution of emission intensity of the $^2H_\alpha$ transition was measured from the spectral features and results are given in Figure 3(b). Emission intensity was calculated from the area under the curve, and intensity was normalized to gate width. The time evolution of $^2H_\alpha$ FWHM is also given in Figure 3(c).

The emission intensity evolution of $^2H_\alpha$ (Figure 3(b)) showed rapid reduction at early times (1 - 5 μs) followed by a slower decay (from 5 - 30 μs). FWHM (Figure 3(c)) showed a similar decay trend with time after the plasma onset. FWHM reaches a minimum value of $\approx$ 30 pm at 30 μs after plasma onset. In addition to instrumental broadening ($\approx$ 13 pm for the detection system used here), several line-broadening mechanisms contribute to the measured line widths reported in Figure 3(c), including Doppler, Stark, and fine and hyperfine structures.

3.2. Double pulse plasma characterization

In the present study, we used an orthogonal reheating scheme where the first pulse is used to ablate the target (ablation pulse), and the second pulse is used to generate a breakdown plasma and reheat the first plume (reheating pulse). The spectrally-resolved $^{1,2}H_\alpha$ emission images (Figure 2(b)) show that the emission predominantly occurs closer to the target. Hence the reheating beam was positioned $\approx$ 1.5 mm away from the target surface where a significant population of H species exists. The parameters of interest for DP LIBS optimization include the interpulse delay (IPD) between ablation and reheating pulses, the energy of the reheating laser, and the pressure of the ambient gas. Thus, a parametric study was carried out to evaluate these parameters.

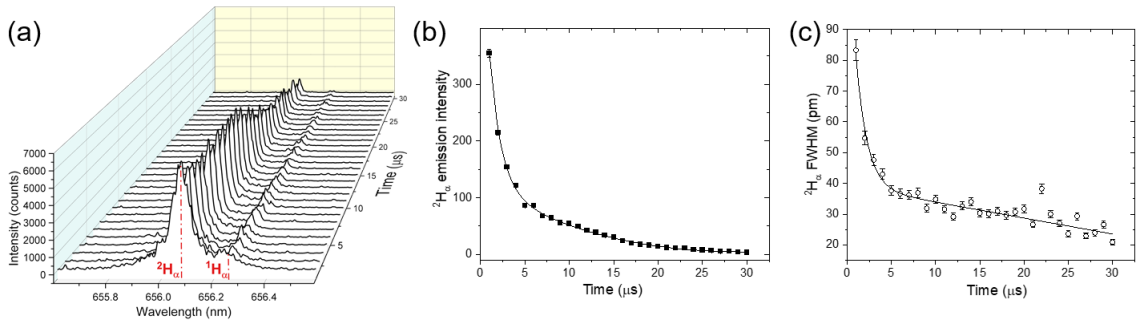

Figure 3: (a) Time-resolved optical emission spectral features generated via SP LIBS, and corresponding (b) $^2H_\alpha$ emission intensity, and (c) $^2H_\alpha$ FWHM. Emission spectral features given in (a) were collected using a progressive gate width from 2 - 10 μs for gate delays from 1 to 30 μs. Emission intensity given in (b) is the area under the $^2H_\alpha$ peak from spectra reported in (a) and is normalized to gate width. Data were collected using 50 mJ for ablation in a 75 Torr He environment.

3.2.1. Influence of interpulse delay

IPD is the most important parameter that influences the analytical merit of a DP LIBS scheme. So, the spectral signatures were collected by varying the IPDs. IPDs ranging from 0 ns to 1500 ns were tested. Examples of spectral evolution with time for an IPD of 500 ns is given in Figure 4(a). The laser energies used for the ablation (first) pulse and reheating pulse were 50 mJ and 500 mJ, respectively. The measurements were carried out at an ambient He gas pressure of 75 Torr. Trends in $^2H_\alpha$ emission intensity as a function of time for IPDs 500 ns and 1000 ns are summarized in Figure 4(b). At an optimal IPD (500 ns), the $^2H_\alpha$ signal increases initially and peaks at $\approx$ 5 μs and then decays. Instead at 1000 ns IPD, the signal decay follows a similar trend to the SP case reported in Figure 3(b). The emission signal levels in the case of the optimal IPD showed a signal enhancement at all times during the time decay compared to the 1000 ns IPD and SP. The variation of ^2H signal intensity with IPD is given in Figure 4(c) which highlights the optimal IPD is $\approx$ 400-500 ns. The measured FWHM values for various 500 ns and 1000 ns IPDs are given in Figure 4(d). At earlier times in plasma evolution, the FWHM for IPD of 500 ns is $\approx$ 20% greater than that for 1000 ns, however by 20 μs after plasma onset, FWHM values are the same for both IPDs.

3.2.2. The role of heating pulse energy

The energy of the reheating pulse may affect the properties of the DP LIBS plume. Hence, the laser energy of the reheating pulse was varied for the orthogonal DP scheme by keeping constant ablation pulse energy (50 mJ). Figure 5(a) shows representative spectral features recorded with varying reheating pulse laser energies (150 mJ, 300 mJ, and 600 mJ). The delay and gate width used for the measurement were 6 μs and 10 μs respectively. The He background pressure was kept at 75 Torr. From the spectral features reported in Figure 5(a), we find that at lower laser energies (e.g., 150 mJ) there is no observable signal enhancement obtained with the DP scheme. As the heating laser energy is increased, significant $^2H_\alpha$ emission signal enhancement is observed. This trend is also reported in Figure 5(b) which compares $^2H_\alpha$ emission intensity for SP and DP schemes for varying heating laser energies. Here, it is clear that signal enhancement is observed when the reheating laser energies are $\geq$ 200 mJ, and there is an approximately linear relationship between $^2H_\alpha$ emission intensity and reheating laser pulse energy.

The observation of a laser energy threshold for observing the signal enhancement indicates the minimum energy required for forming He breakdown plasma (which is shown in Figure 1(b)) in the DP experiments. In Figure 5(c), the measured FWHMs with varying reheating pulse energy are given. FWHM values for DP and SP schemes show that only a marginal increase in FWHM is measured with increasing reheating pulse energy when compared to the SP case. The maximum FWHM measured for the DP scheme is $\approx$40 pm, which is still narrow enough to easily separate $^2H_\alpha$ and $^1H_\alpha$ lines given that the isotopic shift is $\approx$ 180 pm. Lastly, we evaluated the enhancement factor between DP and SP schemes, with results given in Figure 5(d). The enhancement factor is simply the $^2H_\alpha$ intensity for the DP scheme divided by that for the SP scheme. The greatest enhancement is possible at higher laser energies, although at the higher laser energies, some minimal increase in line broadening is observed, as shown in Figure 5(c).

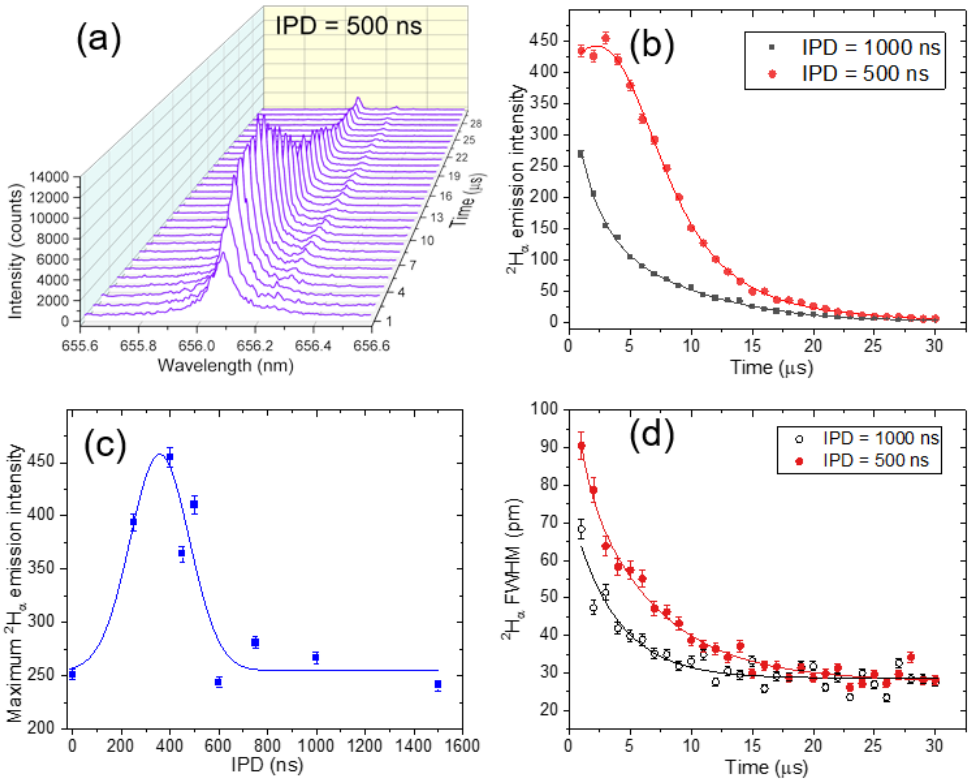

Figure 4: (a) Time-resolved spectral features for an IPD of 500 ns. Emission spectral features were collected using a progressive gate width from 2 - 10 μs for gate delays from 1 to 30 μs. (b) Emission intensity as a function of time for IPDs of 500 and 1000 ns. Emission intensity is the area under the $^2H_\alpha$ peak. (c) Maximum $^2H_\alpha$ intensity as a function of IPD, and (d) FWHM as a function of time after plasma onset. Data reported in (b) and (c) are normalized to gate width. Data were collected using 50 mJ for ablation, and 500 mJ for heating in a 75 Torr He environment.

3.2.3. He ambient pressure effects

Varying He ambient gas pressure was also evaluated to understand its impact on $^2H_\alpha$ emission intensity and FWHM. Figure 6(a) reports example emission spectra collected for varying He gas pressures, for a constant ablation laser energy of 50 mJ, heating laser energy of 500 mJ, at a gate delay/width of 6 μs/ 10 μs, and a constant IPD of 500 ns. Results reported in Figure 6(a) and (b) show there is a threshold phenomenon for signal enhancement; the presence of a He breakdown plasma is needed for signal enhancement in the case of DP. The laser energy required for breakdown plasma formation depends strongly on the pressure as higher energy pulses are required for lower pressure levels [37].

From the spectral features (Figure 6(a)), we find that at pressure 30 Torr, no change between SP and DP schemes is observed. In contrast, at pressures of 75 Torr He and higher, with increasing pressure, we observe increasing signal enhancement along with increased line broadening. For the SP case, as He pressure is increased above 75 Torr, we see a decrease in $^2H_\alpha$ intensity due to the increased cooling at higher He background pressures. Line broadening for the DP experiments does increase approximately nearly with the He pressure, however, even at 110 Torr, both $^2H_\alpha$ and $^1H_\alpha$ lines are separable. Enhancement factor (Figure 6(d)) is also considered for increasing He pressure, and we find an approximately exponential growth is observed. As with all isotopic analysis, there is a trade-off between increasing signal intensity and line broadening.

3.2.4. Analytical merits

Lastly, we compared the analytical merits of DP to those of the SP scheme. Several Zircaloy-4 samples with varying ^2H concentrations were analyzed, and calibration curves were generated for SP and DP schemes, with results reported in Figure 7. To generate the calibration curve, three duplicate spectra were saved (each averaged over 10 shots) per Zircaloy-4 sample so that an average and standard deviation of $^2H_\alpha$ emission intensity (calculated from the area under a Voigt fit of

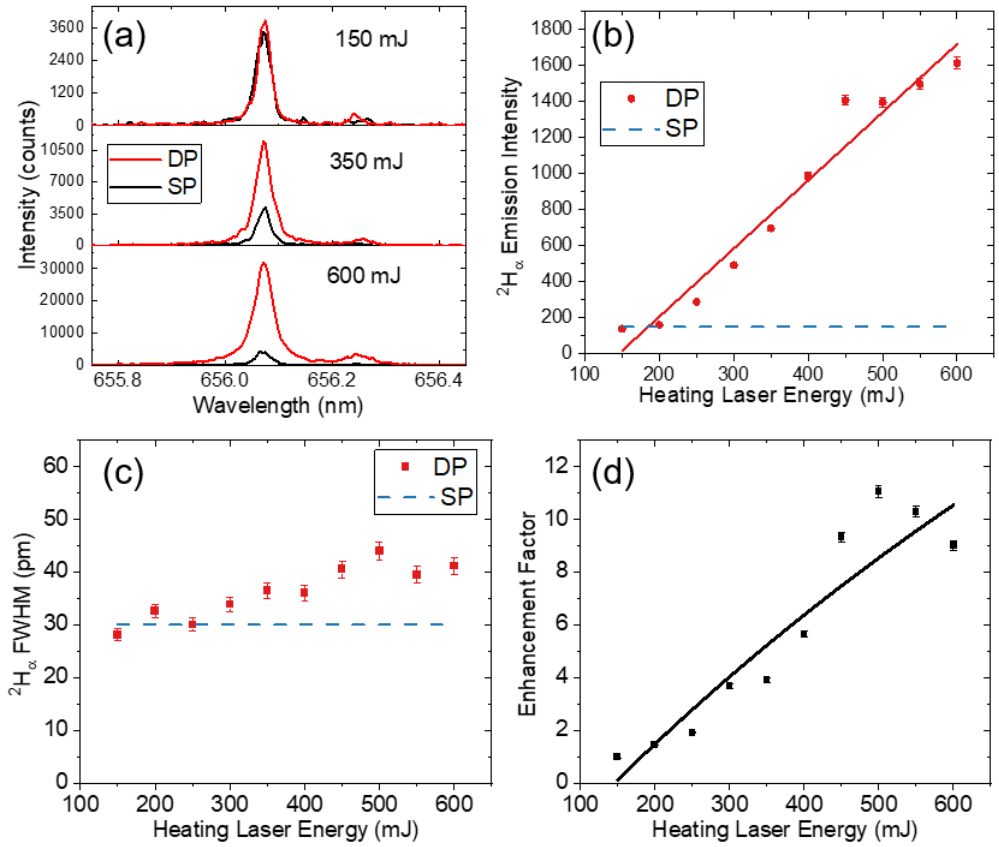

Figure 5: (a) Emission spectra for varying heating laser energies for both SP and DP schemes. (b) $^2H_\alpha$ emission intensity and (c) $^2H_\alpha$ FWHM plotted as a function of heating laser energy, and (d) emission intensity enhancement factor. Data were collected using 50 mJ for ablation, varying heating laser energies, IPD of 500 ns, in a 75 Torr He environment. All measurements were taken at a gate delay/width of 6 μs/ 10 μs.

the $^2H_\alpha$ curve) could be calculated and plotted versus known ^{2}H concentration. This 'known' concentration was determined via weight gain measurements before and after the ^{2}H absorption process described in Section 2 [22]. Y error bars represent the standard deviation between three duplicate $^2H_\alpha$ emission intensity measurements of 10 laser shots each. The measurements were carried out at a He background pressure of 75 Torr, IPD of 500 ns, and with ablation and reheating pulse energies of 50 mJ and 500 mJ, respectively. The gate delay and width for all measurements were 6 μs/ 10 μs.

For the SP case, the $^2H_\alpha$ emission intensity appears to increase rapidly with increasing ^{2}H concentration, and level-off or saturate at higher concentrations ($\approx$40 at. % ^{2}H). This saturation in emission intensity with increasing analyte concentration is indicative of self-absorption. In contrast, for the DP case, a linear relationship is observed, where $^2H_\alpha$ emission intensity increases with increasing ^{2}H concentration. This result suggests that self-absorption is not present or is insignificant when an orthogonal DP experimental set-up is used, using parameters (i.e., IPD, heating laser energy, He gas pressure) that lead to significant signal enhancement and minimal line broadening. It is important to note that although differences are observed between the DP and SP calibration curves, significant scatter is observed for the $^2H_\alpha$ emission intensity values for both schemes. Additional samples over this concentration range would need to be prepared and evaluated to examine the source of this scatter better.

4. Discussion

The present study evaluated the potential of using the DP orthogonal scheme to improve the analytical and detection capabilities of LIBS for hydrogen isotopic analysis. An optimization parametric study was carried out by varying critical parameters affecting the signal intensity, and linewidth, such as IPD, heating pulse energy,

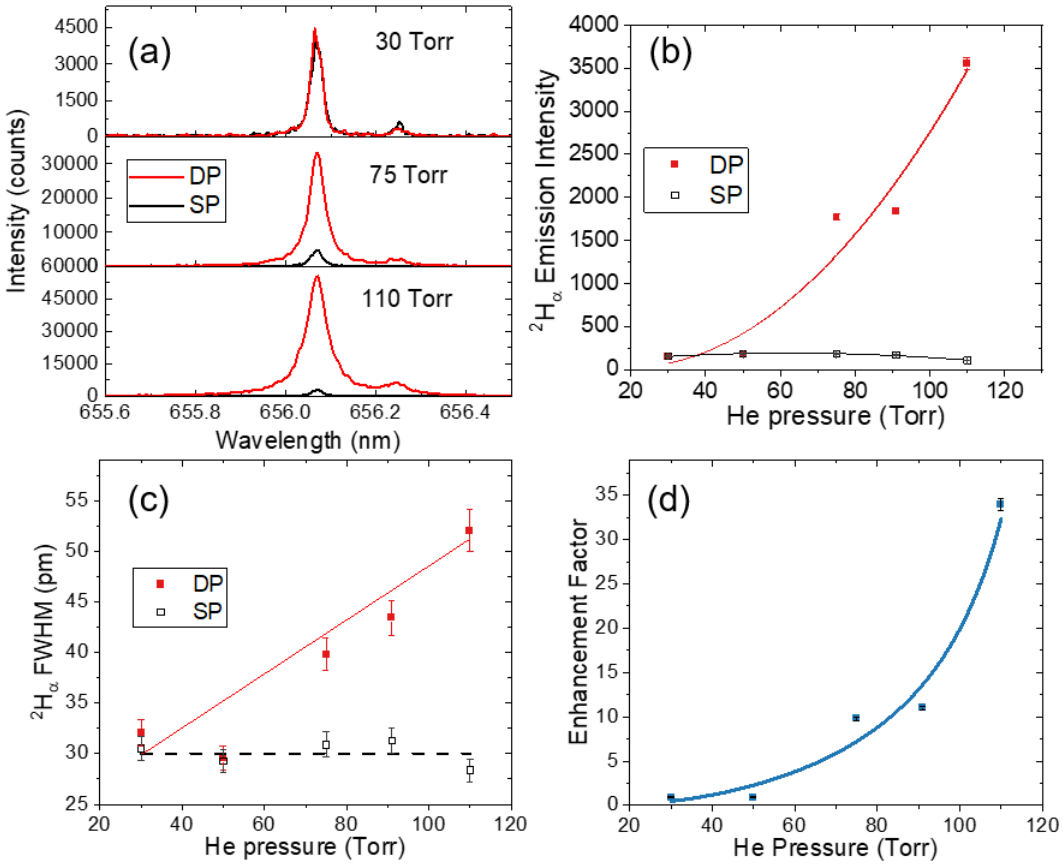

Figure 6: (a) Emission spectra for varying He gas pressures for both SP and DP schemes. (b) $^2H_\alpha$ emission intensity, (c) $^2H_\alpha$ FWHM plotted as a function of He gas pressure (Torr), and (d) emission intensity enhancement factor. Data were collected using 50 mJ for ablation, 500 mJ for heating, IPD of 500 ns, in variable pressure He gas environments. All measurements were taken at a gate delay/width of 6 μs/ 10 μs.

and ambient gas pressure (here, He). Our results highlight that the orthogonal DP scheme is useful in providing signal enhancement and overcoming self-absorption issues at high concentrations of ^{2}H in Zircaloy-4 samples.

Time-resolved 2D spectrally-integrated and spectrally-resolved images of Zircaloy-4 plasma given in Figure 2 showed plume morphology and distribution of $^2H_\alpha$ species. The spectrally-resolved images showed $^2H_\alpha$ emission predominantly occur closer to the target. LPP is an in-homogeneous medium where hotter and denser conditions exist closer to the target [38]. The upper energy level of $^2H_\alpha$ species is $\approx$ 12.09 eV and it indicates higher temperature conditions are required for emission from $^{1,2}H_\alpha$. This is consistent with previous reports which highlighted that the H_α emission predominantly occurs at early times of LPP evolution [17]. The images also showed plume splitting which is anticipated when the LPPs are produced under a moderate ambient pressure environment [39].

The time evolution of H_α linewidth showed the minimum value $\approx$ 30 pm, although the spectrograph resolution was $\approx$ 13 pm. The linewidth of a transition in a LPP is primarily influenced by Stark and Doppler broadening [10]. In addition to these, various line artifacts such as self-absorption and self-reversal may also influence the linewidth. Among these, the Stark broadening, which has a linear dependence on electron density for H transitions, will be predominant at early times of plasma evolution. Being the lightest element in the periodic table, the Doppler broadening is also significant for H emission lines. For example, the Doppler and Stark widths for H_α will be $\approx$ 20 pm and $\approx$ 80 pm respectively for a plasma with a temperature and electron density of $\sim$ 5000 K and $\sim 10^{15}$ cm^{-3} respectively [38]. It indicates that optimal plasma and detection conditions must be selected to minimize the linewidth of the transition for isotopic analysis of H.

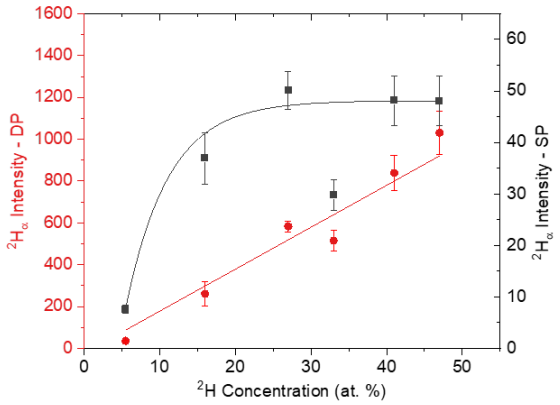

Figure 7: Calibration curve for SP and DP experimental set-ups. Spectral data were collected using 50 mJ for ablation, 500 mJ for heating, IPD of 500 ns, in a 75 Torr He gas environment, at a gate delay/width of 6 μs/ 10 μs.

Although the LIBS technology possesses several advantages over other analytical tools (e.g., ICP-MS), such as rapid and multi-elemental detection, standoff capability, etc., it is much less sensitive, making trace detection difficult. In addition, self-absorption in LPPs may be present, especially when the analyte concentration is high [40]. The DP method is capable of addressing both of these limitations. Several DP schemes have been proposed previously, including collinear, orthogonal reheating, orthogonal pre-ablation LIBS, and DP crossed beam LIBS [36], all of which are useful for enhancing the LIBS signal intensity [41, 42]. The mechanisms leading to signal enhancement in collinear DP scheme were discussed in detail in the literature, and include reheating of the plasma, higher mass ablation rate, and larger plasma volume [43, 44]. DP collinear geometry was commonly used to improve the signal intensity in LIBS. However, collinear geometry may lead to further ablation from the target leading to a denser plasma with higher number density of analyte in the plume, which can lead to a higher degree of self-absorption [45]. So, in the present work, the orthogonal reheating scheme was selected for H_α signal enhancement where the reheating pulse did not interact with the target, thereby preventing further ablation of the target.

We also noticed that the presence of He breakdown plasma is required to see H signal enhancement. For example, the He pressure and energy dependence studies showed that the minimum ambient He pressure and laser energy for the signal enhancement is $\geq$ 75 Torr and $\geq$ 200 mJ. It indicates the approximate laser breakdown threshold for He plasma formation for the pressure used. Higher laser intensities are required for generating breakdown plasma at reduced pressure levels as the threshold laser intensity for gas breakdown follows $I_{th} \propto 1/P^{\alpha}$ where α varies between 0 and 1 [46]. Additionally, for fixed laser energy, the energy absorbed by the gas decreases with gas pressure along with the reduction of the size of the breakdown plasma and its electron number density [47].

The time-integrated images (see Figure 1) showed that plasma volume is significantly higher in the case of the DP orthogonal scheme. However, the linewidth measurements showed only a marginal increase in DP compared to SP for moderate He background pressures. The marginal rise in linewidth could be related to an increase in temperature due to Doppler instead of the Stark effect since the DP measurements were taken at later times of plasma evolution. The reheating of a low-density pre-plasma using high-temperature He breakdown plasma leads to a plasma with a larger volume, eventually reducing self-absorption.

Burger *et al.*[19] noticed an optimum delay of around 50 ns for obtaining the highest H_α signal enhancement for DP collinear experiments using deuterated water. However, the optimal inter-pulse delay in the present experiment employing an orthogonal DP scheme is $\approx$ 500 ns. At lower or higher inter-pulse delays, the signal enhancement is reduced. In an ideal scenario, the optimal inter-pulse delay should provide a reduction in Stark broadening and increase plasma temperature to improve the analyte signal. Since the reheating plasma is generated at a certain distance from the target, the efficient coupling of both plasmas takes place only after a short delay, considering the plume propagation time.

A study comparing the emission signal with reheating laser energy showed ^{2}H signal enhanced linearly with reheating pulse energy after the He breakdown plasma formation. Results also highlight that the background signal does not increase with increasing the heating pulse energy and a marginal increase in linewidth. A signal enhancement of 10 $\times$ is observed when the reheating laser pulse energy is increased from 200 mJ to 600 mJ. Since the reheating pulse is not interacting with the target (no additional ablation), the rapid rise in signal intensity with laser energy could be directly related to the re-excitation of the lower-level population, and the marginal rise in linewidth could be caused by Doppler broadening.

The He pressure dependence study showed significant signal enhancement when the He pressure increased from 20 Torr to 100 Torr (enhancement factor $\approx 10\times$). However, the linewidth of the ^{2}H also increased by a factor of $\approx$ 2. An increase in ambient gas pressure may lead to increased energy absorption

by the breakdown plasma along with electron density. Glumac and Elliott [47] noticed that the electron density of the gas breakdown plasma increases roughly linearly with ambient pressure for a fixed laser energy. The $^2H_\alpha$ linewidth also showed an approximately linear dependence when the He gas pressure increased from 50 to 110 Torr (Figure 6(c)).

The emission intensity of ^{2}H with concentration showed a saturation tendency for the SP case, indicating self-absorption. Numerous parameters influence self-absorption in a LPP and is a complex phenomenon [43]. Some of the experimental parameters that influence self-absorption include laser (wavelength, pulse width, and energy), and environmental conditions (nature and pressure of the gas) and all these are entangled in dictating the thermodynamic conditions and hence the population distribution of various species in a plasma. Also, self-absorption depends strongly on the spectroscopic property of the selected transition (energy of the lower level, degeneracy, and transition probability); hence, it varies with line selection of the same species. In addition, acquisition parameters (delay time and gate width) and mode of light collection (spatially-integrated, spatially-resolved analysis, and angle of observation) may influence self-absorption in a transition. Although H_α is not a resonance line (10.2-12.09 eV), it possesses a very high transition rate (A= 1.324e+08/s), and hence self-absorption could be present at high analyte concentrations [22]. Some of the methods for reducing self-absorption include using lower laser energy for ablation (for reducing the analyte number density) and using reduced environmental pressure conditions due to the rapid expansion of the plume. In the present experiment, a relatively lower pulse energy is used for generating the plasma (50 mJ) along with moderate He ambient pressure conditions (< 100 Torr). However, self-absorption is still evident in the ^{2}H signal intensity at higher analyte concentration levels.

In the present work, the DP LIBS scheme is effective for overcoming the self-absorption in the H_α transition indicated by a linear fit given in Figure 7. Previous studies employing the DP scheme showed mixed results in overcoming self-absorption in LIBS [48–51]. However, most of the DP schemes used collinear geometry where both the plasma generating and reheating pulses approach the target in the same direction and are separated in time. For example, Corsi *et al.* [51] noticed a reduction in self-absorption in Cu and Zn neutral lines in brass plumes while using a collinear geometry. Instead, some other works employing collinear DP showed an increase in self-absorption [49] and even the occurrence of self-reversal [48]. The differences in self-absorption in various collinear schemes could be related to the selection of pre-pulse and heating pulse laser energies and the interaction of the second pulse with the target, leading to an increase in analyte concentration in the plume.

The present work used an orthogonal heating scheme where the second pulse generates a He breakdown plasma (see Figure 1). The optimal interpulse delay was found to be $\approx$ 500 ns. Also, note that significantly higher laser energies were used for breakdown plasma generation compared to ablation pulse energy. The interaction of the ablation plume with the hotter He gas breakdown plume at optimal time delay leads to a larger plume, as indicated in the time-integrated images with additional re-excitation, which reduces self-absorption. The presence of metastable helium atoms in the He breakdown plasma is also expected to play an important role as an excitation energy source for ^{2}H emission [21].

5. Conclusions

LIBS was performed using single and double-pulsing schemes for the purpose of H isotopic detection in Zircaloy-4 target materials. For the DP set-up, an orthogonal re-heating configuration was employed. Critical parameters including IPD, heating laser energy, and He gas pressure were all studied to understand their impact on $^2H_\alpha$ emission intensity and line broadening (i.e., FWHM of $^2H_\alpha$). We found that using an IPD of 400 - 500 ns leads to significant signal enhancement. In the orthogonal DP scheme, the reheating pulse does not interact with the target, hence the measured $^2H_\alpha$ signal enhancement is not due to any further ablation of the target material. We observed that a He breakdown plasma is required to see $^2H_\alpha$ signal enhancement and the changes in emission intensity and linewidth for DP scheme are directly related to the properties of the He breakdown plasma generated. When heating laser energy was varied, we found that for energies greater than 200 mJ, $^2H_\alpha$ emission intensity increased linearly with heating laser energy for the DP case with minimal line broadening. However, an increase in line broadening is noticed for DP with increasing He gas pressure. Lastly, by generating a calibration curve from six Zircaloy-4 samples with varying ^{2}H concentrations (ranging from $\approx$ 5 - 47 at. %), the DP scheme leads to an approximately linear relationship between $^2H_\alpha$ emission intensity and known ^{2}H concentration. The presence of this linear relationship suggests self-absorption is absent, in particular compared to the SP scheme where $^2H_\alpha$ emission intensity saturates at higher ^{2}H concentrations. Hence our results suggest that a DP-LIBS scheme

with optimal IPD, heating laser energy, and He ambient gas pressure, self-absorption can be mitigated, thereby improving the analytical merits of traditional SP LIBS.

Acknowledgments

The authors acknowledge the National Nuclear Security Administration (NNSA) Tritium Modernization Program for financially supporting this work. All work reported in this study was performed at Pacific Northwest National Laboratory, which is operated for the U.S. DOE by Battelle Memorial Institute under Contract No. DE-AC05-76RLO1830.

Declaration of Competing Interests

The authors declare that they have no known competing financial interests or personal relationships that could have appeared to influence the work reported in this paper.

References

[1] H. J. Van Der Meiden, S. Almaviva, J. Butikova, V. Dwivedi, P. Gasior, W. Gromelski, A. Hakola, X. Jiang, I. Jõgi, J. Karhunen, et al. Monitoring of tritium and impurities in the first wall of fusion devices using a LIBS based diagnostic. *Nuclear fusion*, 61(12):125001, 2021.

[2] Y. Huang, W. Liu, S. Wu, Y. Zeng, Y. Qian, Y. Li, and D. Xiao. Control and monitoring of tritium in molten salt reactor. *Nuclear Techniques*, 34(8):632–636, 2011.

[3] C. W. Forsberg, S. Lam, D. M. Carpenter, D. G. Whyte, R. Scarlat, C. Contescu, L. Wei, J. Stempien, and E. Blandford. Tritium control and capture in salt-cooled fission and fusion reactors: status, challenges, and path forward. *Nuclear Technology*, 197 (2):119–139, 2017.

[4] R. Fantoni, S. Almaviva, L. Caneve, F. Colao, G. Maddaluno, P. Gasior, and M. Kubkowska. Hydrogen isotope detection in metal matrix using double-pulse laser-induced breakdown-spectroscopy. *Spectrochim. Acta B*, 129:8–13, 2017.

[5] C.H. Skinner, D. P. Stotler, H. Adler, and A. T. Ramsey. Spectroscopic diagnostics of tritium recycling in tftr. *Rev. Sci. Instrum.*, 66(1):646–648, 1995.

[6] K. A. Burns, E. F. Love, and C. K. Thornhill. Description of the tritium-producing burnable absorber rod for the commercial light water reactor. Technical report, Pacific Northwest National Lab.(PNNL), Richland, WA (United States) PNNL-22086, 2012.

[7] S. S. Harilal, A. K. Shaik, E. J. Kautz, A. Devaraj, A. Casella, and D. Senor. Detection of tritium using ultrafast laser-induced breakdown spectroscopy. *J. Anal. Atom. Spectrom.*, 39(3):699, 2024.

[8] H. B. Andrews, J. McFarlane, and K. G. Myhre. Monitoring noble gases (Xe and Kr) and aerosols (Cs and Rb) in a molten salt reactor surrogate off-gas stream using laser-induced breakdown spectroscopy (libs). *Applied Spectroscopy*, 76(8):988–997, 2022.

[9] G. S. Maurya, A. Marín-Roldán, P. Veis, A. K. Pathak, and P. Sen. A review of the LIBS analysis for the plasma-facing components diagnostics. *Journal of Nuclear Materials*, 541: 152417, 2020.

[10] S. S. Harilal, B. E. Brumfield, N. L. LaHaye, K. C. Hartig, and M. C. Phillips. Optical spectroscopy of laser-produced plasmas for standoff isotopic analysis. *Applied Physics Reviews*, 5(2): 021301, 2018.

[11] E. J. Kautz, A. Xu, A. V. Harilal, M. P. Polek, A. M. Casella, D. J. Senor, and S. S. Harilal. Influence of ambient gas on self-reversal in li transitions relevant to isotopic analysis. *Optics Express*, 31(3):3549–3564, 2023.

[12] J. Wu, Y. Qiu, X. Li, H. Yu, Z. Zhang, and A. Qiu. Progress of laser-induced breakdown spectroscopy in nuclear industry applications. *Journal of Physics D: Applied Physics*, 53(2): 023001, 2019.

[13] A. P. Rao, P. R. Jenkins, R. E Pinson, J. D. Auxier II, M. B Shattan, and A. K. Patnaik. Machine learning in analytical spectroscopy for nuclear diagnostics. *Applied Optics*, 62(6):A83–A109, 2023.

[14] E. J. Kautz, E. N. Weerakkody, M. S. Finko, D. Curreli, B. Koroglu, T. P. Rose, D. G. Weisz, J. C. Crowhurst, H. B. Radousky, M. DeMagistris, et al. Optical spectroscopy and modeling of uranium gas-phase oxidation: Progress and perspectives. *Spectrochimica Acta Part B: Atomic Spectroscopy*, 185:106283, 2021.

[15] E. H. Kwapis, J. Borrero, K. S. Latty, H. B. Andrews, and K. C. Hartig. Laser ablation plasmas and spectroscopy for nuclear applications. *Applied Spectroscopy*, 78(1):9–55, 2024.

[16] M. Burger, L. A. Finney, L. Garrett, S. S. Harilal, K. C. Hartig, J. Nees, P. J. Skrodzki, X. Xiao, and I. Jovanovic. Laser ablation spectrometry for studies of uranium plasmas, reactor monitoring, and spent fuel safety. *Spectrochim. Acta B*, 179: 106095, 2021.

[17] E. J. Kautz, A. Devaraj, D. J. Senor, and S. S. Harilal. Hydrogen isotopic analysis of nuclear reactor materials using ultrafast laser-induced breakdown spectroscopy. *Optics Express*, 29(4): 4936–4946, 2021.

[18] H. Suyanto, Z. S. Lie, H. Niki, K. Kagawa, K. Fukumoto, H. Rinda, S. N. Abdulmadjid, A. M. Marpaung, M. Pardede, M. M. Suliyanti, et al. Quantitative analysis of deuterium in zircaloy using double-pulse laser-induced breakdown spectrometry and helium gas plasma without a sample chamber. *Analytical chemistry*, 84(5):2224–2231, 2012.

[19] M. Burger, P. J. Skrodzki, L. A. Finney, J. Hermann, J. Nees, and I. Jovanovic. Isotopic analysis of deuterated water via single-and double-pulse laser-induced breakdown spectroscopy. *Physics of Plasmas*, 25(8):093103, 2018.

[20] Elizabeth J Kautz, David J Senor, and Sivanandan S Harilal. The interplay between laser focusing conditions, expansion dynamics, ablation mechanisms, and emission intensity in ultrafast laser-produced plasmas. *Journal of Applied Physics*, 130(20), 2021.

[21] M . Pardede, T. J. Lie, J. Iqbal, M. Bilal, R. Hedwig, M. Ramli, A. Khumaeni, W. S. Budi, N. Idris, S. N. Abdulmadjid, et al. H-D analysis employing energy transfer from metastable excited-state he in double-pulse libs with low-pressure he gas. *Analytical chemistry*, 91(2):1571–1577, 2018.

[22] E. J. Kautz, E. Ronnebro, A. Devaraj, D. Senor, and S. S. Harilal. Detection of hydrogen isotopes in zircaloy-4 via femtosecond LIBS. *J. Anal. Atom. Spectrom.*, 36:1217, 2021.

[23] C. G. Parigger, D. M. Surmick, G. Gautam, and A. M. El Sherbini. Hydrogen alpha laser ablation plasma diagnostics. *Optics Letters*, 40(15):3436–3439, 2015.

[24] Y. Ikeda, J. K. Soriano, N. Kawahara, and I. Wakaida. Spatially

and temporally resolved plasma formation on alumina target in microwave-enhanced laser-induced breakdown spectroscopy. *Spectrochim. Acta B*, 197:106533, 2022.

[25] E. J. Kautz, M. C. Phillips, and S. S. Harilal. Laser-induced fluorescence of filament-produced plasmas. *J. Appl. Phys.*, 130 (20), 2021.

[26] I. Karnadi, M. Pardede, I. Tanra, R. Hedwig, A. M. Marpaung, Z. S. Lie, E. Jobiliong, D. Kwaria, M. M. Suliyanti, M. Ramli, et al. Suppression of self-absorption in laser-induced breakdown spectroscopy using a double pulse orthogonal configuration to create vacuum-like conditions in atmospheric air pressure. *Scientific reports*, 10(1):13278, 2020.

[27] J. L. Gottfried, F. C De Lucia Jr., C. A. Munson, and A. W. Miziolek. Strategies for residue explosives detection using laser-induced breakdown spectroscopy. *J. Anal. Atom. Spectrom.*, 23 (2):205–216, 2008.

[28] B. C. Windom, P. K. Diwakar, and D. W. Hahn. Dual-pulse laser induced breakdown spectroscopy for analysis of gaseous and aerosol systems: plasma-analyte interactions. *Spectrochim. Acta B*, 61(7):788–796, 2006.

[29] A. De Giacomo, M. Dell'Aglio, F. Colao, and R. Fantoni. Double pulse laser produced plasma on metallic target in seawater: basic aspects and analytical approach. *Spectrochim. Acta B*, 59 (9):1431–1438, 2004.

[30] A. Casavola, A. De Giacomo, M. Dell'Aglio, F. Taccogna, G. Colonna, O. De Pascale, and S. Longo. Experimental investigation and modelling of double pulse laser induced plasma spectroscopy under water. *Spectrochim. Acta B*, 60(7-8):975–985, 2005.

[31] V. Lazic, J. J. Laserna, and S. Jovicevic. Insights in the laser induced breakdown spectroscopy signal generation underwater using dual pulse excitation - part ii: Plasma emission intensity as a function of interpulse delay. *Spectrochim. Acta B*, 82:50–59, 2013.

[32] G. Nicolodelli, G. S. Senesi, R. A. Romano, I. L. de Oliveira Perazzoli, and Debora M. Bastos P. M. Signal enhancement in collinear double-pulse laser-induced breakdown spectroscopy applied to different soils. *Spectrochim. Acta B*, 111:23–29, 2015.

[33] M. Cui, Yoshihiro Deguchi, C. Y., Z. Wang, S. Tanaka, and D. Zhang. Carbon detection in solid and liquid steel samples using ultraviolet long-short double pulse laser-induced breakdown spectroscopy. *Spectrochim. Acta B*, 167, 2020.

[34] N. Giannakaris, A. Haider, C. M. Ahamer, S. Grünberger, S. Trautner, and J. D. Pedarnig. Femtosecond single-pulse and orthogonal double-pulse laser-induced breakdown spectroscopy (libs): Femtogram mass detection and chemical imaging with micrometer spatial resolution. *Applied Spectroscopy*, 76(8): 926–936, 2022.

[35] A. De Giacomo, M. Dell'Aglio, D. Bruno, R. Gaudiuso, and O. De Pascale. Experimental and theoretical comparison of single-pulse and double-pulse laser induced breakdown spectroscopy on metallic samples. *Spectrochim. Acta B*, 63(7):805–816, 2008.

[36] P. K. Diwakar, S. S. Harilal, J. R. Freeman, and A. Hassanein. Role of laser pre-pulse wavelength and inter-pulse delay on signal enhancement in collinear double-pulse laser-induced breakdown spectroscopy. *Spectrochim. Acta B*, 87:65–73, 2013.

[37] C. V. Bindhu, S. S. Harilal, M. S. Tillack, F. Najmabadi, and A. C. Gaeris. Laser propagation and energy absorption by an argon spark. *J. Appl. Phys.*, 94(12):7402–7407, 2003.

[38] S. S. Harilal, M. C. Phillips, D. H. Froula, K. K. Anoop, R. C. Issac, and F. N. Beg. Optical diagnostics of laser-produced plasmas. *Reviews of Modern Physics*, 94(3):035002, 2022.

[39] S. S. Harilal, C. V. Bindhu, M.S. Tillack, F. Najmabadi, and A.C. Gaeris. Internal structure and expansion dynamics of laser ablation plumes into ambient gases. *J. Appl. Phys.*, 93(5):2380–2388, 2003.

[40] Heh-Young Moon, Kathleen K Herrera, Nicoló Omenetto, Benjamin W Smith, and James D Winefordner. On the usefulness of a duplicating mirror to evaluate self-absorption effects in laser induced breakdown spectroscopy. *Spectrochimica Acta Part B: Atomic Spectroscopy*, 64(7):702–713, 2009.

[41] A Guarnaccio, GP Parisi, D Mollica, Angela De Bonis, Roberto Teghil, and A Santagata. Fs–ns double-pulse laser induced breakdown spectroscopy of copper-based-alloys: Generation and elemental analysis of nanoparticles. *Spectrochimica Acta Part B: Atomic Spectroscopy*, 101:261–268, 2014.

[42] A Santagata, Roberto Teghil, G Albano, D Spera, P Villani, Angela De Bonis, GP Parisi, and Agostino Galasso. fs/ns dual-pulse libs analytic survey for copper-based alloys. *Applied Surface Science*, 254(4):863–867, 2007.

[43] F. Rezaei, G. Cristoforetti, E. Tognoni, S. Legnaioli, V. Palleschi, and A. Safi. A review of the current analytical approaches for evaluating, compensating and exploiting self-absorption in laser-induced breakdown spectroscopy. *Spectrochim. Acta B*, 169:105878, 2020.

[44] E. Tognoni and G. Cristoforetti. Basic mechanisms of signal enhancement in ns double-pulse laser-induced breakdown spectroscopy in a gas environment. *J. Anal. Atom. Spectrom.*, 29(8): 1318–1338, 2014.

[45] F Bredice, FO Borges, H Sobral, M Villagran-Muniz, Héctor Oscar Di Rocco, G Cristoforetti, S Legnaioli, V Palleschi, L Pardini, A Salvetti, et al. Evaluation of self-absorption of manganese emission lines in laser induced breakdown spectroscopy measurements. *Spectrochimica Acta Part B: Atomic Spectroscopy*, 61(12):1294–1303, 2006.

[46] P. Chylek, M. A. Jarzembski, V. Srivastava, and R. G. Pinnick. Pressure dependence of the laser-induced breakdown thresholds of gases and droplets. *Applied optics*, 29(15):2303–2306, 1990.

[47] N. Glumac and G. Elliott. The effect of ambient pressure on laser-induced plasmas in air. *Opt. Las. Engg.*, 45:27–35, 2007.

[48] C. Gautier, P. Fichet, D. Menut, J. Lacour, D. L'Hermite, and J. Dubessy. Main parameters influencing the double-pulse laser-induced breakdown spectroscopy in the collinear beam geometry. *Spectrochim. Acta B*, 60(6):792–804, 2005.

[49] F. Bredice, F. O. Borges, H. Sobral, M. Villagran-Muniz, H.. O. Di Rocco, G. Cristoforetti, S. Legnaioli, V. Palleschi, L. Pardini, A. Salvetti, et al. Evaluation of self-absorption of manganese emission lines in laser-induced breakdown spectroscopy measurements. *Spectrochim. Acta B*, 61(12):1294–1303, 2006.

[50] A. M. El Sherbini, T. M. El Sherbini, H. Hegazy, G. Cristoforetti, S. Legnaioli, V. Palleschi, L. Pardini, A. Salvetti, and E. Tognoni. Evaluation of self-absorption coefficients of aluminum emission lines in laser-induced breakdown spectroscopy measurements. *Spectrochim. Acta B*, 60(12):1573–1579, 2005.

[51] M. Corsi, G. Cristoforetti, M. Giuffrida, M. Hidalgo, S. Legnaioli, V. Palleschi, A. Salvetti, E. Tognoni, and C. Vallebona. Three-dimensional analysis of laser-induced plasmas in single and double pulse configuration. *Spectrochim. Acta B*, 59(5): 723–735, 2004.